

RESEARCH ARTICLE

Plasma-sprayed TiO₂ coatings: Hydrophobicity enhanced by ZnO additions

Yusliza Yusuf¹  | Mariyam Jameelah Ghazali² | Jariah Mohamad Juoi³ |
Toibah Abd Rahim³ | Zaleha Mustafa³

¹ Fakulti Teknologi Kejuruteraan Mekanikal dan Pembuatan, Universiti Teknikal Malaysia Melaka, Durian Tunggal, Malaysia

² Centre for Materials Engineering and Smart Manufacturing, Faculty of Engineering and Built Environment, Universiti Kebangsaan Malaysia, Bangi, Malaysia

³ Fakulti Kejuruteraan Pembuatan, Universiti Teknikal Malaysia Melaka, Durian Tunggal, Malaysia

Correspondence

Yusliza Yusuf, Fakulti Teknologi Kejuruteraan Mekanikal dan Pembuatan, Universiti Teknikal Malaysia Melaka, Hang Tuah Jaya, 76100 Durian Tunggal, Melaka, Malaysia.

Email: yusliza@utem.edu.my

Mariyam Jameelah Ghazali, Centre for Materials Engineering and Smart Manufacturing, Faculty of Engineering and Built Environment, Universiti Kebangsaan Malaysia, 43600 UKM Bangi, Selangor, Malaysia.

Email: mariyam@ukm.edu.my

Funding information

Ministry of Higher Education Malaysia, Universiti Kebangsaan Malaysia, Grant/Award Number: FRGS/1/2018/TK03/UKM/02/8; Universiti Teknikal Malaysia Melaka internal, Grant/Award Number: PJP/2020/FTKMP/PP/S01737

Abstract

Titanium dioxide (TiO₂) powder mixed individually with 10 and 30 weight percentage (wt%) ZnO was thermally sprayed onto a grade B API 5 L carbon steel substrate by atmospheric plasma spraying. The effect of the addition of ZnO (10 wt% and 30 wt%) on the microstructures and wettability properties of the TiO₂/ZnO coatings was investigated. The characterization of the coatings was carried out using scanning electron microscopy, X-ray diffraction (XRD), laser confocal microscope, and sessile droplet system. The XRD analysis of the coating revealed that the anatase phase of TiO₂ in the powder state transformed into rutile phases for the produced TiO₂/ZnO coatings. Surface microstructure analysis revealed that the coatings had typical micro-roughened surfaces of plasma spraying products. The coating with 30 wt% ZnO produced a coating with remarkable pores and microcracks compared with the TiO₂ coating and coating with 10 wt% ZnO. Additionally, the increase in the wt% of ZnO increased the surface roughness value of the produced coatings and substantially changed the wettability properties of the TiO₂ coating from hydrophilic to hydrophobic.

KEYWORDS

TiO₂/ZnO coating, wettability properties

1 | INTRODUCTION

Titanium dioxide (TiO₂) coatings are widely used in biomedical applications and self-cleaning coatings owing to their wear and corrosion resistance, and

biocompatibility.^{1–4} However, TiO₂ coatings have drawbacks, such as failure caused by bacterial infection in biomedical applications,⁵ and TiO₂ photocatalytic activity is limited within the visible region owing to low sunlight absorption.^{6–8} Hence, various methods have

been tested to overcome this problem, including mixing with different oxides such as zirconium oxide (ZrO_2) and stannic oxide (SnO_2) to increase the photocatalytic activity of TiO_2 .^{9,10} Recently, TiO_2 coatings mixed with zinc, silver, and copper were established to improve the coatings' photocatalytic and antibacterial activity.^{2,9,11} Zinc oxide (ZnO) is an interesting alternative to TiO_2 for enhanced photocatalytic and antibacterial activity because it has lower cost and better photocatalytic activity compared with other metal oxides, and high efficiency in the processing and isolation of the electron-hole pairs for photocatalytic applications that minimize bacterial infection.^{12–14} Additionally, ZnO is often selected owing to its superior advantages, including low cost, high quantum efficiency, environmental efficiency, biodegradability, and ease of alteration, in various microstructures.^{15,16} Moreover, TiO_2 and ZnO have very similar physicochemical properties, including nontoxicity, thermal and chemical stability, biocompatibility, and mechanical strength.¹⁵ To date, few studies have investigated the combination of TiO_2 and ZnO , although the ratio of ZnO plays a vital role in the photocatalytic and structural characteristics.^{17–19} Furthermore, Moradi et al.¹⁷ reported that the addition of ZnO to TiO_2 restricts light penetration and decreases the photocatalytic activity. Tian et al.²⁰ observed poor crystallization and cracks on the generated film when the ZnO content was higher. Moreover, Zhao, Peng, and You (2017) reported that the addition of ZnO alters the topography of the TiO_2 coatings, which may be beneficial for improving the biological performance.

Several methods for generating TiO_2/ZnO ceramic coatings using distinct TiO_2 and ZnO precursors have recently been proposed. These techniques include sol-gel,^{20,21} electrospinning,^{22,23} and chemical co-precipitation.¹⁸ All of these techniques require precise synthesis control to achieve materials with beneficial properties. The produced coating exhibits various physicochemical properties and structures depending on the process parameters. However, the production of TiO_2/ZnO coatings using plasma spraying technology has rarely been reported, particularly for TiO_2/ZnO coatings using micro-sized feed powder in the spraying process. The plasma spraying process is widely used to fabricate metallic and ceramic coatings for wear resistance, corrosion resistance, and thermal barrier applications. Therefore, in this study, we attempted to produce a TiO_2/ZnO coating on a carbon steel substrate with a 10 wt% and 30 wt% ratio of ZnO using atmospheric plasma spraying systems. The objective was to investigate the effect of ZnO addition on the surface characteristics of the generated coating in terms of the surface coating microstructure and morphology, surface roughness, and wettability properties. The resultant TiO_2/ZnO coating is expected to

TABLE 1 Process parameters of atmospheric plasma spraying

Parameter	Value
Arc current (A)	600
Primary gas argon (psi)	80
Secondary gas helium (psi)	40
Carrier gas argon (psi)	30
Powder feed rate (rpm)	4
Spraying distance (mm)	80
Robot speed (mm/s)	250
Preheat (cycle)	2

be useful in mechanical industries that require antifouling and self-cleaning qualities that are consistent with the original features of TiO_2 and ZnO .

2 | MATERIALS AND METHODS

In this study, a commercially available TiO_2 powder, namely, Metco 102 from Oerlikon Metco (≥ 99 wt%, particle size of 11–65 μm), and ZnO powder supplied by Sigma Aldrich (≥ 99 wt%, particle size ≤ 25 μm) were used as the basic materials. The TiO_2 powders were mixed and reconstituted as feedstock powders for the plasma spraying process with the addition of 10 wt% and 30 wt% ZnO . During the mixing phase, 50 ml of deionized (DI) water was mixed with 100 g of powder. The mixture was milled for 2 h, dried for 24 h at 80°C, and sieved using 80-mesh sieves. The powder particle size analysis of the prepared feedstock powders was conducted using the Mastersizer Malvern Instrument. The powder particle morphology was investigated using scanning electron microscopy (SEM, Zeiss Leo 1450VP).

Then, using an atmospheric plasma spray device (SG-100 torch, Praxair, USA), the TiO_2/ZnO ceramic coatings were deposited onto a grade B API 5 L carbon steel substrate with the size of 30 cm (length) \times 5 cm (width) \times 7 mm (thickness). Before the spraying process, the substrates were sandblasted using a 24-mesh aluminium grit and ultrasonically cleaned in ethanol and DI water. The dried substrate was sprayed with plasma under the parameters listed in Table 1.

The crystalline structures of all obtained TiO_2/ZnO ceramic coatings were analyzed by X-ray diffraction (XRD, X'pert-Pro system) with a $CuK\alpha$ radiation wavelength of $\lambda = 1.5406$ Å. The X-ray data were collected at a scanning step size of $.05^\circ$ over the 2θ range of 20–70°. The surface morphologies of the coatings and the cross-sectioned region were observed by SEM (Zeiss Leo 1450VP), and the surface roughness (Ra) was investigated using an Olympus LEXT OLS4000 laser confocal microscope. A

1024 × 1024 μm image of the coated sample's surface was scanned, and the roughness profile was measured using a 405-nm laser. The arithmetic mean surface roughness property (Ra) parameter values were recorded in this investigation. To acquire an accurate assessment for each sample, an average of three surface roughness values was taken. Porosity analysis on the different SEM images captured at different coating locations was carried out using the ImageJ software based on ASTM E2109-01 standard. The coating's cross-sectional image was observed using an SEM (Zeiss LEO 1450VP) at a magnification of 100X at several different random areas. The observed cross-sectional surface images were then analyzed using computer software to determine the average porosity percentage.

For the wettability test, static contact angle (CA) imaging and the angle measurement of the TiO₂/ZnO ceramic coatings were carried out using a sessile droplet system at ambient temperature and humidity. The static CA was measured by placing a 1.0-μL sessile droplet of water on the sample surface. The images were captured and analyzed to calculate the CA. A high-speed camera (EasyDrop Kruss GmbH) was used for the CA measurement. Image analysis and measurements were carried out using the DSA1 software.

3 | RESULTS AND DISCUSSION

3.1 | TiO₂/ZnO as feed powders for plasma spraying

Figure 1 shows the SEM images of the feed powders used in this study. The coarse TiO₂ as-received powder exhibits a typical morphology for the fused and crushed powders (Figure 1A). The as-received ZnO powder used in this study contained uniformly rounded particles, as shown in Figure 1B. Figure 1C,D shows the ZnO (small particle) uniformly attached to the TiO₂ particles after the mixing process and reconstituted as feedstock powders for the plasma spraying process. After the milling process, the particle size of the TiO₂ particle decreased by approximately 50% from $d(.5) = 32.7 \mu\text{m}$ to $d(.5) = 15.7 \mu\text{m}$ and $16.4 \mu\text{m}$ for the samples with 10 wt% ZnO and 30 wt% ZnO, respectively.

In the plasma spraying process, the powder morphology and homogeneity of the particle composition are crucial for the coating behavior, particularly at high temperatures.²⁴ The flow ability of the powders through the injection system is affected by the shape and uniformity of the particles. Owing to the weak flow ability, the rate of powder feed is unstable, which results in inhomogeneous coating structures.²⁴ The angular particles of the as-received TiO₂ powder used in this study had a large surface area, and their plane faces provided an extensive con-

tact area with the adjacent particles.²⁴ Therefore, the angular particles increased the inter-particle friction forces, and the wear of the feeding systems increased during milling and thereby eased the inclusion of ZnO into TiO₂. Moreover, the high surface-to-volume ratio of the synthesized TiO₂/ZnO angular particles increased the potential reactions with warm gases or the vaporization during plasma spraying, which led to the increase of the finishing pores and pore content in the produced coatings.²⁵

3.2 | XRD analysis, microstructure morphology, and surface roughness investigations of TiO₂/ZnO coatings

Figure 2 shows the XRD analysis of the as-received TiO₂ powder, as-received ZnO powder, TiO₂ coating, TiO₂-90 wt%/ZnO-10 wt% coating, and TiO₂-70 wt%/ZnO-30 wt% coating. The majority of rutile phase was observed in this study for TiO₂ in the powder state, as well as anatase phase (Figure 2A). The anatase phase in the powder state transformed into rutile phases for the TiO₂/ZnO coatings produced. For the peaks at $2\theta = 35.09^\circ$, 44.21° , and 54.54° (Figure 2A), the anatase phase has transformed into rutile for the TiO₂ coating produced (Figure 2C). According to other studies, the anatase phase is irreversibly transformed into rutile at the temperatures of 500–600°C.²⁶ In this study, the transformation of the anatase phase to rutile was caused by the high temperature during the plasma spraying process, which resulted from the plasma melting the feed powder during the deposition process at temperatures exceeding 600°C. In turn, this resulted in the observed phases of the TiO₂ ceramic coating being mainly titania rutile (JCPDS 00-21-1276) planes (Figure 2C). The rutile peaks of the TiO₂-90 wt%/ ZnO-10 wt% ceramic coating and TiO₂-70 wt%/ ZnO-30 wt% ceramic coating slightly shifted to a greater angle compared with the TiO₂ ceramic coating (Figure 2D,E). These results were further supported by the values of 2θ and d-spacing together with their respective lattice structures of significant peaks of TiO₂/ ZnO coatings as given in Table 2. Peak shifts to greater angles are generally a result of defect relaxation and stress, as well as changes in the stoichiometry and chemical composition.²⁷ Additionally, the unit cell parameter (Table 3) indicates that the TiO₂ rutile structure decreases by approximately .33 percent when ZnO is added. This is most likely due to the components being mixed together. A mixture of ZnO in a lower concentration than the TiO₂ base material will occupy an interstitial position, altering the lattice structure and increasing the XRD diffraction angle.

Additionally, the sharp diffraction peak of the TiO₂ ceramic coating indicates the high crystallinity of

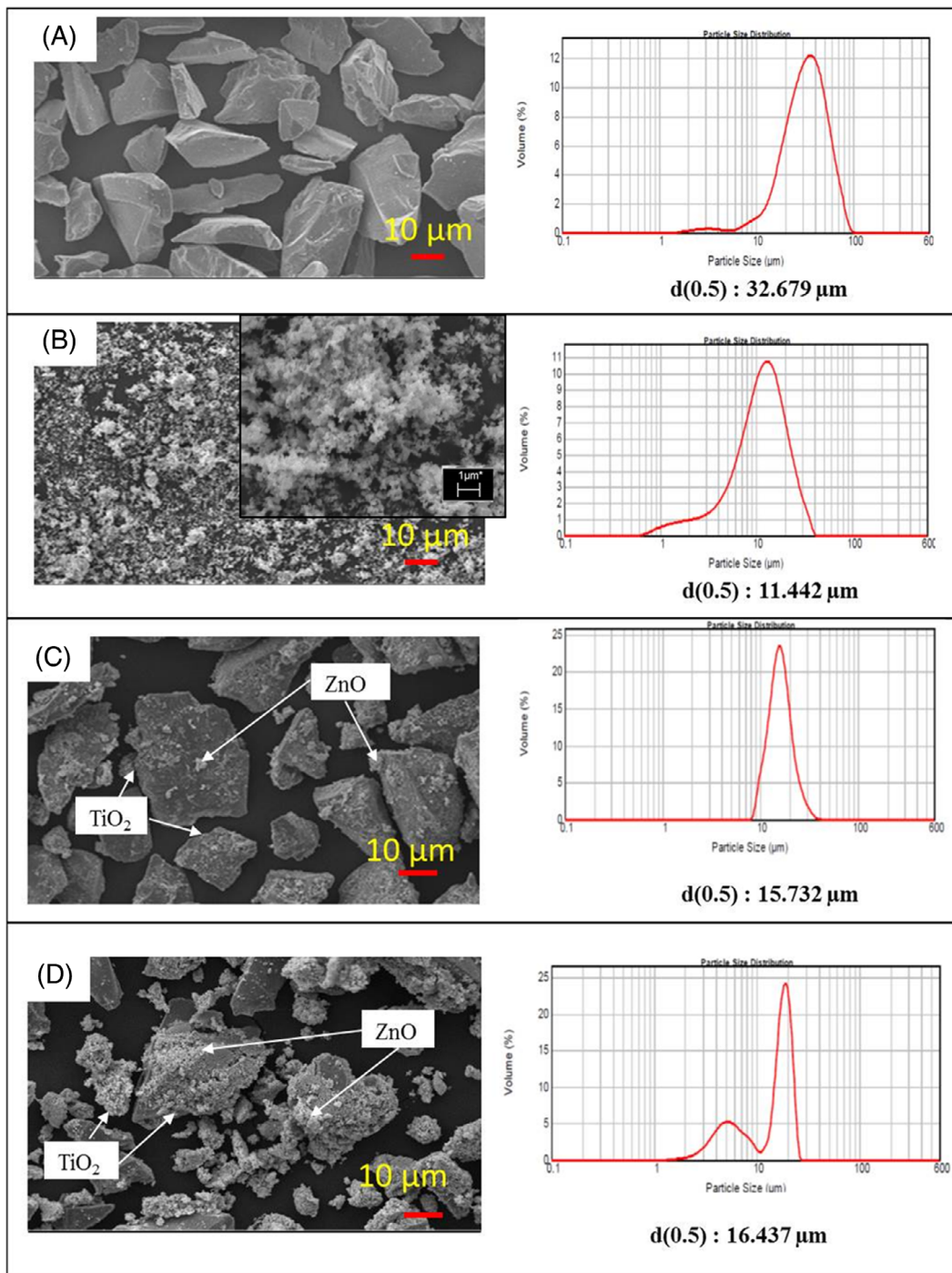


FIGURE 1 Scanning electron microscopy (SEM) images of feedstock powders: (A) as-received TiO_2 powder with $d(0.5)$ particle size of $32.679 \mu\text{m}$; (B) as-received ZnO powder with $d(0.5)$ particle size of $11.442 \mu\text{m}$; (C) mixture of 10 wt% ZnO + 90 wt% TiO_2 powder with $d(0.5)$ particle size of $15.732 \mu\text{m}$; (D) mixture of 30 wt% ZnO + 70 wt% TiO_2 powder with $d(0.5)$ particle size of $16.437 \mu\text{m}$

TiO_2 , which is attributed to the high purity of TiO_2 (Figure 2C,D). However, the intensity of the major titania diffraction peak of the TiO_2 -70 wt%/ ZnO -30 wt% coating decreased when the ZnO content increased (Figure 2E). This indicates that the presence of ZnO in the resulting coating did not change the rutile phase of TiO_2 , owing to the lower ZnO content used in this study.

Figure 3 shows the SEM micrographs of the surface and cross-section images of the TiO_2/ZnO coatings at various wt% ZnO . As can be seen, all produced coatings consisted of fully melted and unmelted areas, which later developed a rough surface as shown in the SEM surface images. Typical micro-roughened surfaces, which are characteristic of plasma spraying products owing to

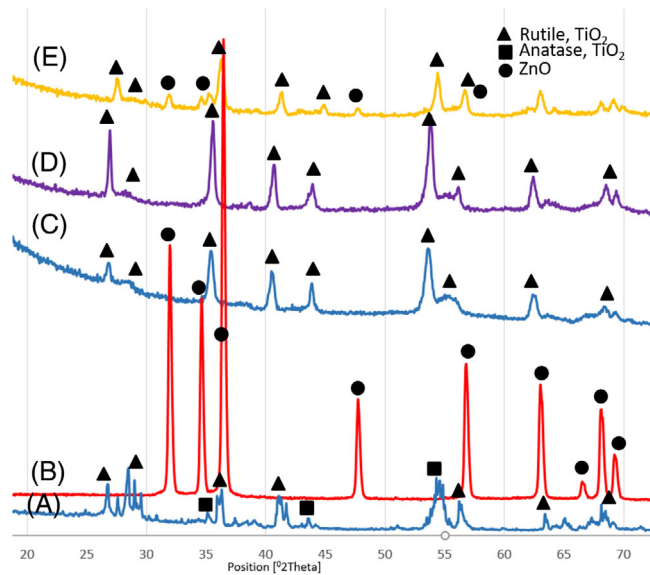


FIGURE 2 X-ray diffraction (XRD) patterns of (A) as-received TiO_2 powder; (B) as-received ZnO powder; (C) TiO_2 coating; (D) TiO_2 -90 wt%/ZnO-10 wt% coating; (E) TiO_2 -70 wt%/ZnO-30 wt% coating

TABLE 2 Values of 2θ , d-spacing, and lattice structure of significant peaks of TiO_2 /ZnO coatings

Coating	2θ	d-spacing (Å)	hkl
TiO_2 coating	27.464	3.245	110
	36.056	2.489	101
	41.226	2.188	111
	54.337	1.687	211
	56.631	1.624	220
	68.999	1.360	301
TiO_2 -90 wt%/ZnO-10 wt% coating	27.472	3.244	110
	36.095	2.486	101
	41.208	2.189	111
	54.343	1.687	211
	56.7	1.622	220
	68.982	1.360	301
TiO_2 -70 wt%/ZnO-30 wt% coating	27.552	3.235	110
	36.095	2.486	101
	41.258	2.186	111
	54.393	1.685	211
	56.65	1.623	220
	68.982	1.360	301

the high-enthalpy plasma jet, were applied, and melting accelerated to form solidified splats on the substrate corresponding to the melted areas during the spraying process.²⁶ Additionally, small pores were discovered on the surface of the coating, which is attributed to unmelted

TABLE 3 Lattice parameters for the rutile structures

Sample	Lattice parameters (Å)	
	$a = b$	c
TiO_2 coating	4.589	2.96
TiO_2 -90 wt%/ZnO-10 wt% coating	4.587	2.95
TiO_2 -70 wt%/ZnO-30 wt% coating	4.574	2.95

particles. Figure 3B,C shows the surface microstructure for ZnO additions with different wt%. As the ZnO wt% content increased, significant pores on the surface were clearly observed (Figure 3C). Additionally, numerous surface microcracks were observed as the ZnO content (wt%) increased. The TiO_2 -70 wt%/ZnO-30 wt% sample had remarkable microcracks and pores on the surface (Figure 3C). Similar observations were made for the coatings in the cross-section images. Coating with 30 wt% ZnO resulted in remarkable pores and lower thickness compared with TiO_2 -90 wt%/ZnO-10 wt% and TiO_2 coating.

In this study, the development of a microcrack may have been caused by the combination of the TiO_2 /ZnO matrix reinforcement and unmelted particles. The use of ZnO powder with a greater specific density (5.61 g/cm^3) compared with that of TiO_2 (4.23 g/cm^3) is considered to have resulted in the formation of pores and microcracks. Additionally, the high specific density of the ZnO powder used in this analysis resulted in speed delay for particles approaching the substrate's surface during the spraying process. Therefore, a higher wt% ZnO addition resulted in the formation of pores and microcracks, and in the decrease of coating thickness as the wt% ZnO concentration increased. This is evident in the SEM image of the cross-section of the TiO_2 /ZnO ceramic coating (Figure 3).

The cross-sectional microstructure of the coating exhibited the strong adherence of coating to the substrate (Figure 3). The cross-sectional images show that the TiO_2 ceramic coating was dense and thick compared with the TiO_2 -90 wt%/ZnO-10 wt% and TiO_2 -70 wt%/ZnO-30 wt% samples. The TiO_2 -70 wt%/ZnO-30 wt% sample exhibited a thin coating under the same plasma spraying coating process parameters. Nevertheless, in the SEM cross-sectioned image, the microcracks on the surface of the coating are not visible in the cross-sectional area, which indicates that the resulting coating has good adhesion to the substrate surface. The resulting microcrack was only observed at the top surface area of the coating. This finding is in line with the results of Zhao et al.,² who reported that TiO_2 coatings with the highest ZnO content exhibited uneven and disorderly morphologies owing to the high plasma spraying temperature and rapid cooling rates.

Figure 4 shows the surface roughness (R_a) values of the TiO_2 /ZnO coating at a specific wt% ZnO. All

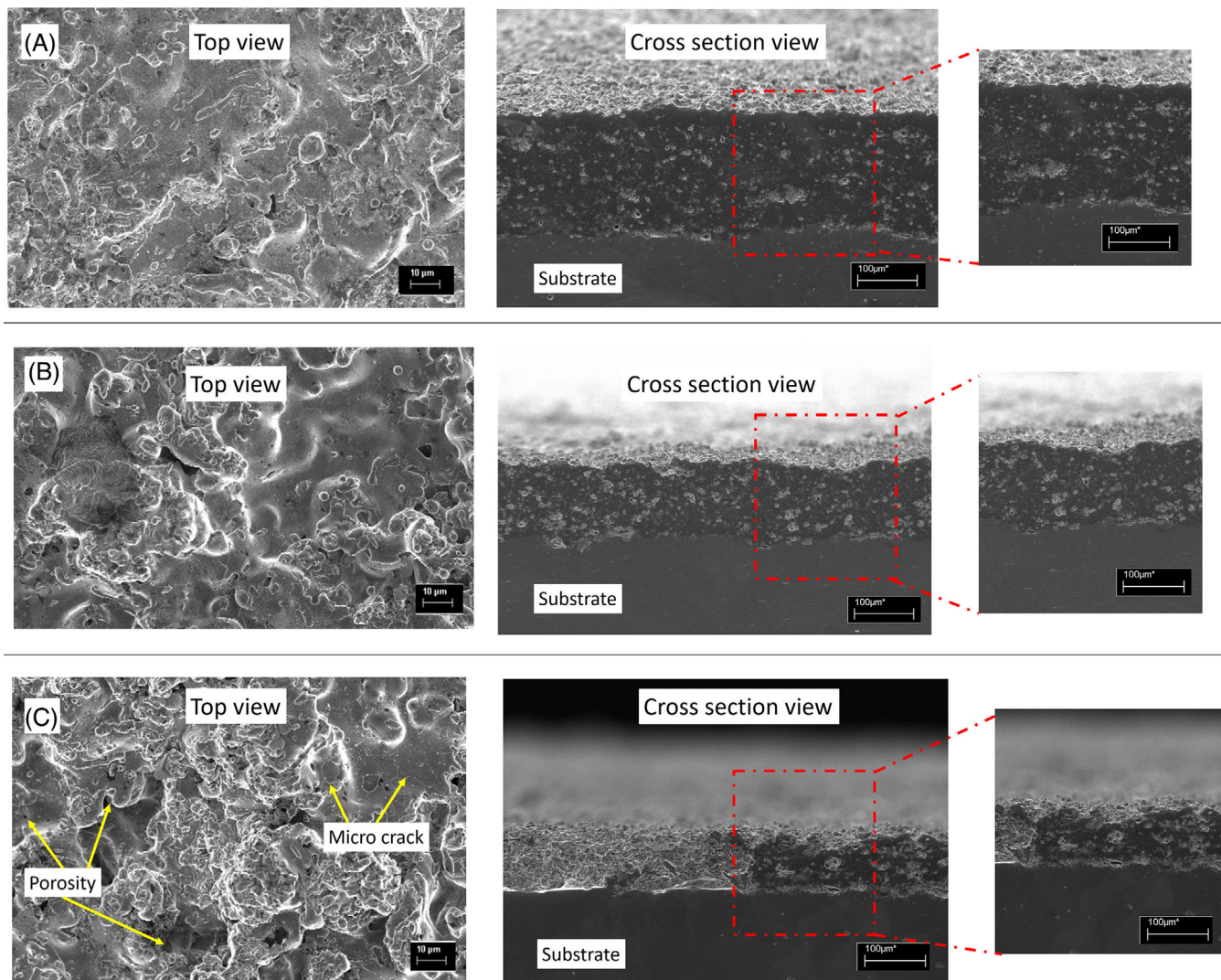


FIGURE 3 Surface and cross section scanning electron microscopy (SEM) images of (A) TiO_2 coating, (B) TiO_2 -90 wt%/ZnO-10 wt% coating, and (C) TiO_2 -70 wt%/ZnO-30 wt% coating

of the developed TiO_2/ZnO coatings have comparable plasma-sprayed roughness values. However, ZnO mixing significantly increased the surface roughness values of the TiO_2 -90 wt%/ZnO-10 wt% and TiO_2 -70 wt%/ZnO-30 wt% coatings compared with the TiO_2 coating. This parameter is associated with the pores and microcracks in the obtained coating. The TiO_2 -70 wt%/ZnO-30 wt% coating exhibited remarkable pores and microcracks and achieved the highest value of $R_a = 6.075 \pm 1.401 \mu\text{m}$. Generally, the influence of surface roughness exerts a significant effect on the coating properties and the coating's functional efficiency, such as wear,²⁸ corrosion,²⁹ magnetism,³⁰ wettability,³¹ and bacterial adhesion.³² In this study, the addition of ZnO to the TiO_2 coating enhanced the surface roughness values and is thought to have affected the wettability properties of the coatings.

3.3 | Porosity analysis of TiO_2/ZnO coatings

Porosity analysis was conducted on 10 different images for each type of produced coating using SEM image analysis and the ImageJ software, as shown in Figure 5. The TiO_2 -70 wt%/ZnO-30 wt% coatings have the highest average porosity percentage at $11.43\% \pm .76\%$, and the TiO_2 -90 wt%/ZnO-10 wt% coatings have an average porosity percentage of $8.01\% \pm .79\%$. These findings are consistent with the observations made in the SEM images shown in Figure 3. The increase of the wt% of the ZnO content in the coating increased the total porosity of the coatings.

In this study, the increasing porosity of the coating surface was caused by the formation of plate coatings on uneven substrate surfaces. The ZnO, which has higher

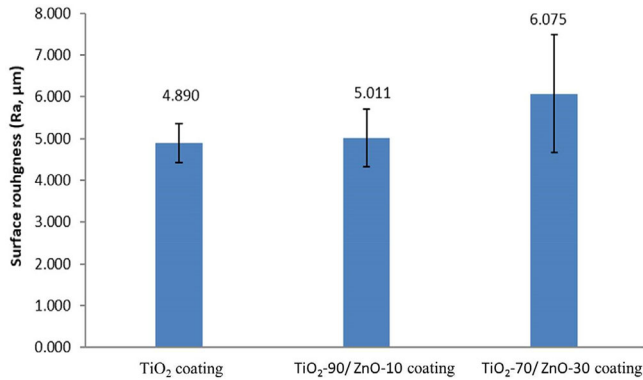


FIGURE 4 Surface roughness (Ra value) of plasma-sprayed TiO₂ coating, TiO₂-90 wt%/ZnO-10 wt% coating, and TiO₂-70 wt%/ZnO-30 wt% coating

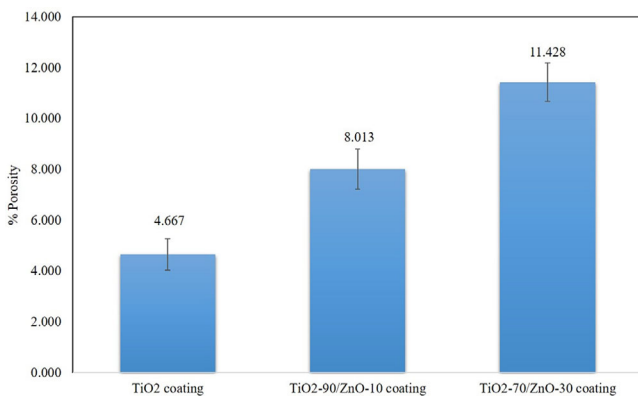


FIGURE 5 Porosity percentage of plasma-sprayed TiO₂ coating, TiO₂-90 wt%/ZnO-10 wt% coating, and TiO₂-70 wt%/ZnO-30 wt% coating

density (5.61 g/cm^3) compared with TiO₂ (4.23 g/cm^3), is believed to delay the particle arrival at the substrate surface during the spraying process, which leads to the trapping of air on the surface and the subsequent emergence of porosity. Additionally, previous studies have shown that

the surface porosity of the coating is formed by trapped air sacs and the process of solidification shrinkage that occurs during the solidification process when the plasma spraying process is carried out.³³ The porosity is formed when the area between the plates is curved and not covered with other particles that are deposited thereafter.

3.4 | Water static CAs analysis

The water static CAs on the TiO₂/ZnO ceramic coating surfaces were investigated to understand the influence of ZnO addition on the wettability of the TiO₂ coatings. As shown in Figure 6, the water CA exhibits hydrophilic surface properties for the TiO₂ ceramic coating sample at $54.1 \pm .17^\circ$. The water CA significantly increased to $100.1 \pm .78^\circ$ after the addition of 10 wt% ZnO, which suggests that the TiO₂-90/ZnO-10 ceramic coating possesses hydrophobic surfaces. The TiO₂-70/ZnO-30 sample also exhibited hydrophobic properties with a CA of $95.4 \pm .46^\circ$. In this study, the hydrophobic surface properties of the TiO₂/ZnO ceramic coatings were determined by the coatings' surface morphology, structure, and coating composition. As shown in Figure 4, the increase of the wt% of the ZnO content tended to increase the coating structure and the surface roughness values. The surface roughness values increased with the generation of micro/nanostructures. Consequently, with a high surface roughness value (TiO₂-70/ZnO-30), the water CA is comparatively high and results in hydrophobicity properties, whereas with a low surface roughness value (TiO₂ coating), the water CA is low, which indicates a coating with high wettability properties. However, there are no clear cut correlations between the surface with high surface roughness properties, and the surface wettability properties were found. For example, in this study the TiO₂-70/ZnO-30 coating shows the highest surface roughness value properties with a CA of $95.4 \pm .46^\circ$ compared to the TiO₂-90/ZnO-10 coating with highest CA

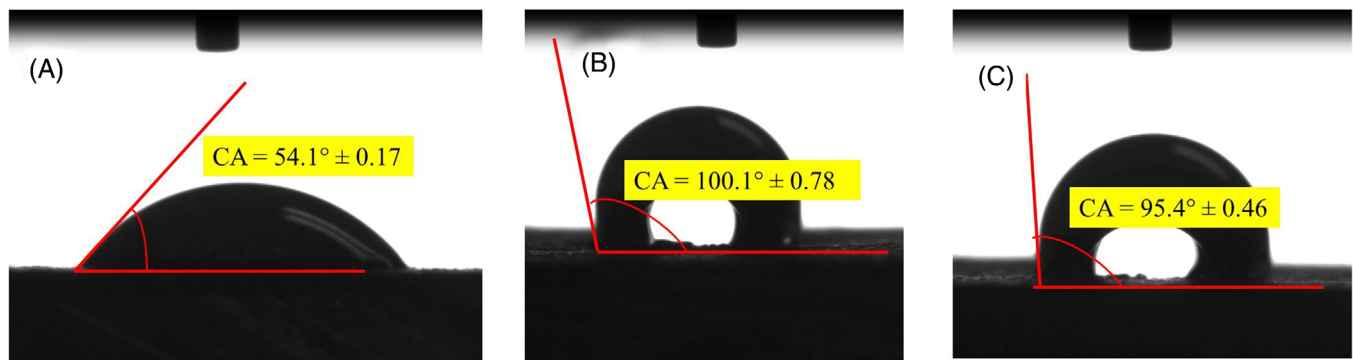


FIGURE 6 Water static contact angle (CA) on (A) TiO₂ coating, (B) TiO₂-90 wt%/ZnO-10 wt% coating, and (C) TiO₂-70 wt%/ZnO-30 wt% coating

of $100.1 \pm .78^\circ$. In this situation, it demonstrates that the coating composition (surface chemistry) is more essential than the surface morphological aspects, as the roughness attributes had no effect on the coating wettability properties. This observation is explained by the fact that the surface chemistry plays a significant role in defining the intrinsic wetting behavior of ideally surfaces.³⁴

According to the Cassie–Baxter model of the wettability of a rough surface, liquid drops cannot reach enough tiny cavities on the surface, and so they lie on the top of the asperities, which results in a composite interface that contains trapped air in the cavities.³⁵ Therefore, rough surface properties consisting of a micro/nanostructure are crucial for achieving hydrophobic performance. To attain the hydrophobic condition, the surface roughness of the material must exceed that of the Cassie–Baxter model, which is considered as a composite film comprising rough surface material, with air trapped in the micro/nanostructured cavities.³⁶ Furthermore, in this study, an increase in the wt% of the ZnO content resulted in the coatings having hydrophobic properties that can improve water resistance.³⁷ The TiO₂ coating reduces the CA and given surface to create a hydrophilic surface that increases the self-cleaning ability.²⁰

4 | CONCLUSION

The plasma spraying method was employed to deposit the TiO₂ coating with 10 wt% and 30 wt% ZnO on a grade B carbon steel substrate. The coating properties associated with long-term performance, such as surface morphology, surface roughness, and wettability, were investigated as a function of the amount of ZnO (wt%) mixed into the TiO₂ ceramic coatings. The addition of 10 wt% and 30 wt% ZnO into the TiO₂ coating did not change the rutile structure of the titania phase. The surface characteristics of all coatings exhibited micro-roughness properties, and the mixing of ZnO at 30 wt% increased the number of remarkable pores observed on the coating, which resulted in high surface roughness. The addition of ZnO to TiO₂ resulted in hydrophobic surface properties.

CONFLICT OF INTEREST

The authors declare that there is no conflict of interest that could be perceived as prejudicing the impartiality of the research reported.

ACKNOWLEDGMENTS

This work was supported by the Ministry of Higher Education Malaysia, Universiti Kebangsaan Malaysia (FRGS/1/

2018/TK03/UKM/02/8), and Universiti Teknikal Malaysia Melaka internal grant (PJP/2020/FTKMP/PP/SO1737). The first author also expresses gratitude to Universiti Teknikal Malaysia Melaka (UTeM) for financially sponsoring her PhD studies.

ORCID

Yusliza Yusuf  <https://orcid.org/0000-0001-8772-4041>

REFERENCES

1. Wen K, Liu M, Liu X, Deng C, Zhou K. Deposition of photocatalytic TiO₂ coating by modifying the solidification pathway in plasma spraying. *Coatings* 2017;7:1–9. <https://doi.org/10.3390/coatings7100169>.
2. Zhao X, Peng C, You J. Plasma-sprayed ZnO/TiO₂ Coatings with enhanced biological performance. *J Therm Spray Technol.* 2017;26:1301–7. <https://doi.org/10.1007/s11666-017-0573-2>.
3. Forghani SM, Ghazali MJ, Muchtar A, Daud AR. Mechanical properties of plasma sprayed nanostructured TiO₂ coatings on mild steel. *Ceram Int.* 2014;40:7049–56. doi:<https://doi.org/10.1016/j.ceramint.2013.12.036>.
4. Forghani SM, Ghazali MJ, Muchtar A, Daud AR, Yusoff NHN, Azhari CH. Effects of plasma spray parameters on TiO₂-coated mild steel using design of experiment (DoE) approach. *Ceram Int.* 2013;39:3121–7. doi:<https://doi.org/10.1016/j.ceramint.2012.09.092>.
5. Jemat A, Ghazali MJ, Razali M, Otsuka Y. Microstructural, surface roughness and wettability of titanium alloy coated by YZP-30wt. % TiO₂ for dental application. *J Teknol.* 2018;80:45–50. doi:<https://doi.org/10.11113/jt.v80.10875>.
6. Du J, Wu Q, Zhong S, Gu X, Liu J, Guo H, et al. Effect of hydroxyl groups on hydrophilic and photocatalytic activities of rare earth doped titanium dioxide thin films. *J Rare Earths.* 2015;33:148–53. doi:[https://doi.org/10.1016/S1002-0721\(14\)60395-1](https://doi.org/10.1016/S1002-0721(14)60395-1).
7. Nakata K, Fujishima A. TiO₂ photocatalysis: design and applications. *J Photochem Photobiol, C.* 2012;13:169–89. doi:<https://doi.org/10.1016/j.jphotochemrev.2012.06.001>.
8. Sopha H, Krbal M, Ng S, Prikryl J, Zazpe R, Yam FK, et al. Highly efficient photoelectrochemical and photocatalytic anodic TiO₂ nanotube layers with additional TiO₂ coating. *Appl Mater Today.* 2017;9:104–10. doi:<https://doi.org/10.1016/j.apmt.2017.06.002>.
9. Meiqing F, Songxia H, Bo R, Xiaoyan J. Synthesis of nanocomposite TiO₂/ZrO₂ prepared by different templates and photocatalytic properties for the photodegradation of Rhodamine B. *Power Technol.* 2013;235:27–32. Doi: <https://doi.org/10.1016/j.powtec.2012.09.042>
10. Nithyadevi D, Rajendrakumar RT. Synthesis, Characterization and photocatalytic properties of TiO₂-SnO₂ composite nanoparticles. *Adv Mater Res.* 2013;678:373–7. Doi: <https://doi.org/10.4028/www.scientific.net/amr.678.373>.
11. Do T-O, Mohan S. Editorial, special issue on “emerging trends in TiO₂ photocatalysis and applications”. *Catalysts* 2020;10:670. doi:<https://doi.org/10.3390/catal10060670>.
12. Navidpour AH, Kalantari Y, Salehi M, Salimijazi HR, Amirnasr M, Rismanchian M, et al. Plasma-sprayed photocatalytic zinc oxide coatings. *J Therm Spray Technol.* 2017;26:717–27. doi:<https://doi.org/10.1007/s11666-017-0541-x>.

13. Jašková V, Hochmannová L, Vyřasová J. TiO₂ and ZnO nanoparticles in photocatalytic and hygienic coatings. *Int J Photoenergy*. 2013;2013:1–6. doi:<https://doi.org/10.1155/2013/795060>.
14. Ogunsona EO, Muthuraj R, Ojogbo E, Valerio O, Mekonnen TH. Engineered nanomaterials for antimicrobial applications: a review. *Appl Mater Today*. 2020;18:100473. doi: <https://doi.org/10.1016/j.apmt.2019.100473>.
15. Samsuri SAM, Rahman MYA, Umar AA, Salleh MM. Effect of zinc acetate dihydrate precursor concentration on the properties of TiO₂-ZnO core-shell nanograss hetero-structure. *J Alloys Compd*. 2015;623:460–5. doi:<https://doi.org/10.1016/j.jallcom.2014.10.192>.
16. Rosnan N, Haan TY, Mohammad AW. Synthesis and characterization of ZnO-decorated GO nanocomposite material with different ZnO loading through sol-gel method. *J Keju-ruter*. 2018;30:249–55. doi:[https://doi.org/10.17576/jkukm-2018-30\(2\)-15](https://doi.org/10.17576/jkukm-2018-30(2)-15).
17. Moradi S, Aberoomand-Azar P, Raeis-Farshid S, Abedini-Khorrami S, Givianrad MH. The effect of different molar ratios of ZnO on characterization and photocatalytic activity of TiO₂/ZnO nanocomposite. *J Saudi Chem Soc*. 2016;20:373–8. doi:<https://doi.org/10.1016/j.jscs.2012.08.002>.
18. Arabnezhad M, Shafiee Afarani M, Jafari A. Co-precipitation synthesis of ZnO–TiO₂ nanostructure composites for arsenic photodegradation from industrial wastewater. *Int J Environ Sci Technol*. 2019;16:463–8. doi:<https://doi.org/10.1007/s13762-017-1585-7>.
19. Siwińska-Stefańska K, Kubiaka A, Piasecki A, Goscianska J, Nowaczyk G, Jurga S, et al. TiO₂-ZnO binary oxide systems: comprehensive characterization and tests of photocatalytic activity. *Materials (Basel)*. 2018;11:1–19. doi:<https://doi.org/10.3390/ma11050841>.
20. Tian J, Chen L, Dai J, Wang X, Yin Y, Wu P. Preparation and characterization of TiO₂, ZnO, and TiO₂/ZnO nanofilms via sol-gel process. *Ceram Int*. 2009;35:2261–70. doi:<https://doi.org/10.1016/j.ceramint.2008.12.010>.
21. Kwiatkowski M, Bezverkhy I, Skompska M. ZnO nanorods covered with a TiO₂ layer: Simple sol-gel preparation, and optical, photocatalytic and photoelectrochemical properties. *J Mater Chem A*. 2015;3:12748–60. doi:<https://doi.org/10.1039/C5TA01087J>.
22. Li W, Wu D, Yu Y, Zhang P, Yuan J, Cao Y, et al. Investigation on a novel ZnO/TiO₂-B photocatalyst with enhanced visible photocatalytic activity. *Phys E Low Dimensional Syst Nanostruct*. 2014;58:118–23. doi:<https://doi.org/10.1016/j.physe.2013.12.004>.
23. Li J, Yan L, Wang Y, Kang Y, Wang C, Yang S. Fabrication of TiO₂/ZnO composite nanofibers with enhanced photocatalytic activity. *J Mater Sci: Mater Electron*. 2016;27:7834–8. doi:<https://doi.org/10.1007/s10854-016-4773-1>.
24. Fauchais P, Montavon G, Bertrand G. From powders to thermally sprayed coatings. *J Therm Spray Technol*. 2010;19:56–80. doi:<https://doi.org/10.1007/s11666-009-9435-x>.
25. Nouri A, Sola A. Powder morphology in thermal spraying. *J Adv Manuf Process*. 2019;1:e10020. doi:<https://doi.org/10.1002/amp2.10020>.
26. Adel AM. Incorporation of nano-metal particles with paper matrices. *Interdiscip J Chem*. 2016;1:36–46. doi:<https://doi.org/10.15761/ijc.1000107>.
27. Iwashita N. X-ray powder diffraction. Beijing, China: Tsinghua University Press Limited; 2016. doi:<https://doi.org/10.1016/B978-0-12-805256-3.00002-7>.
28. Yin B, Zhou HD, Yi DL, Chen JM, Yan FY. Microsliding wear behaviour of HVOF sprayed conventional and nanostructured WC-12Co coatings at elevated temperatures. *Surf Eng*. 2010;26:469–77. doi:<https://doi.org/10.1179/026708410X12506870724352>.
29. Fedrizzi L, Rossi S, Cristel R, Bonora PL. Corrosion and wear behaviour of HVOF cermet coatings used to replace hard chromium. *Electrochim Acta*. 2004;49:2803–14. doi:<https://doi.org/10.1016/j.electacta.2004.01.043>.
30. Ann J, Berndt CC. Surface roughness of plasma sprayed coatings: a statistical approach. *DVS*. 2014;302:599–604.
31. Nakae H, Inui R, Hirata Y, Saito H. Effects of surface roughness on wettability. *Acta Mater*. 1998;46:2313–8. doi:[https://doi.org/10.1016/s1359-6454\(98\)80012-8](https://doi.org/10.1016/s1359-6454(98)80012-8).
32. Costa L, Dantas DM, Silva-Neto JP, Dantas TS, Naves LZ, Domingues F, et al. Bacterial adhesion and surface roughness for different clinical techniques for acrylic polymethyl methacrylate. *Int J Dent*. 2016;2016:8685796.
33. Hajian Foroughani M, Shamanian M, Salehi M, Davar F. Porosity analysis and oxidation behavior of plasma sprayed YSZ and YSZ/LaPO₄ abradable thermal barrier coatings. *Ceram Int*. 2016;42:15868–75. doi:<https://doi.org/10.1016/j.ceramint.2016.07.057>.
34. Yusliza Y, Mariyam JG, Yuichi O, Sarita M, Susumu N, Kiyoshi O, et al. Wettability characteristics of laser surface textured plasma sprayed TiO₂/ZnO coatings. *Tribol Online*. 2019;14:279–84. doi: <https://doi.org/10.2474/trol.14.279>
35. Feng Y, Chen S, Frank Cheng Y. Stearic acid modified zinc nano-coatings with superhydrophobicity and enhanced antifouling performance. *Surf Coat Technol*. 2018;340:55–65. doi:<https://doi.org/10.1016/j.surfcoat.2018.02.053>.
36. Conde JJ, Ferreira-Aparicio P, Chaparro AM. Anti-corrosion coating for metal surfaces based on superhydrophobic electro-sprayed carbon layers. *Appl Mater Today*. 2018;13:100–6. doi:<https://doi.org/10.1016/j.apmt.2018.08.001>.
37. Geetha N, Sivaranjani S, Ayeshamariam A, Kissinger JS, Arasu MV, Jayachandran M. ZnO doped oxide materials: mini review. *Fluid Mech Open Access*. 2016;3:141. doi:<https://doi.org/10.4172/2476-2296.1000141>.

How to cite this article: Yusuf Y, Ghazali MJ, Juoi JM, Rahim TA, Mustafa Z. Plasma-sprayed TiO₂ coatings: Hydrophobicity enhanced by ZnO additions. *Int J Appl Ceram Technol*. 2022;19:2213–2221. <https://doi.org/10.1111/ijac.14009>